Effects of vibration on pool boiling heat transfer from a vertically aligned array of heated tubes

S. M. A. Noori Rahim Abadi[1], A. Ahmadpour[2], J. P. Meyer[*,1]

[1]Department of Mechanical and Aeronautical Engineering, University of Pretoria, Pretoria, South Africa

[2]Department of Mechanical Engineering, Amirkabir University of Technology, Tehran, Iran

[*]Corresponding author's email: josua.meyer@up.ac.za

Tel: +27 0 12 420 3104

Fax: +27 0 12 362 5124

Abstract:

In the present study, the use of mechanical vibration for the enhancement of pool boiling heat transfer is evaluated theoretically. For this purpose, a vertical array of vibrating circular tubes is considered. The array is submerged in a pool of water under atmospheric conditions and electrically heated for boiling to occur on the tube surfaces. To model this phase-change phenomenon, a two-fluid formulation is employed and accompanied by the Rensselaer Polytechnic Institute (RPI) model to estimate the boiling heat flux on a solid surface. A comprehensive parametric study is undertaken to investigate the effects of the amplitude and frequency of vibration, the magnitude of the heat flux, and the pitch-to-diameter ratio of the array on pool boiling heat transfer in the presence of mechanical vibration. An increase of up to 90% in the heat transfer rate is achieved within the simulated operating conditions.

Keywords: Pool boiling, tube array, mechanical vibration, two-fluid formulation.

1. Introduction

Pool boiling is the main heat transfer mechanism in numerous industrial applications including the direct liquid immersion cooling of electronic devices (Alangar, 2017), emergency cooling of nuclear reactors (Schaffrath et al., 1999; Sutharshan et al., 2011) , and large-capacity refrigeration using flooded-type evaporators (Gorgy and Eckels, 2012). The wide use of pool boiling in different heat exchanging apparatuses (some of which are mentioned later) is attributed to the substantial heat transfer rates attained during the pool boiling phase change at low to moderate working temperatures. Enhancement of the pool boiling heat transfer can result in the design and production of more compact and efficient heat exchanging devices, and various techniques have been proposed and examined for this purpose over the last 50 years.

Various techniques, categorized as either passive or active, have been utilized for the augmentation of pool boiling on heated surfaces. The addition of nanoparticles and a surfactant (Shoghl and bahrami, 2013), surface roughening, heated surface enhancement (Stutz et al., 2011; Ustinov et al., 2011), using porous surfaces (Patil and Kandlikar, 2014; Surtaev et al., 2016) and micro/nanostructured boiling surfaces (Kim et al., 2015) are among the various passive techniques. By contrast, the use of electrodynamics (Di Marco and Grassi, 2011) and fluid/surface mechanical vibration (Prinsnyakov et al., 1992) are the most well-known active methods for enhancing the pool boiling heat transfer. Among these various techniques, the vibration of boiling surfaces by an external mechanical exciter has shown to be an extremely effective method for the elevation of the heat transfer coefficient during pool boiling (Prisnyakov and Prisnyakov, 2001). Moreover, flow-induced vibrations in a frequency range of 10–20 Hz are naturally present in heat exchanging devices and can be used effectively to enhance the pool boiling heat transfer without major additional costs.

In a pioneering experimental study, Bergles (1969) addressed the effects of surface vibration on pool boiling heat transfer. A vertically vibrating cylindrical tube was submerged in a pool of distillated atmospheric water and heated using an electrical heater to examine the boiling phenomenon on a vibrating surface. A notable enhancement in the heat transfer rate was reported when the heat flux was relatively low. The same conclusion was drawn by Markov (1980), who studied pool boiling in a heated wire in the presence of vibrations at frequencies of 75–100 Hz.

Vinko and Naim (1994) conducted numerous experiments on pool boiling over horizontal and vertical flat surfaces that were vibrating at an adjustable frequency/amplitude. Water was used as the boiling liquid, and an increase of up to 25% in the heat transfer rate as a result of surface vibration was reported. Moreover, it was revealed that the enhancing effect of mechanical vibration is superior for horizontal surfaces in comparison to vertical surfaces.

In another work, Chou et al. (2002) investigated the effects of vertical vibration of a boiling tank on the amount of vapour generated inside a boiling chamber when several steel balls were added to the system. It was reported that the combination of properly sized steel balls together with mechanical vibration at sufficiently high frequencies resulted in the most efficient boiling scenario. In the best case, a 32% enhancement was observed in the volume fraction of water vapour.

The effects of flow-induced vibrations on the critical heat flux (CHF) were investigated by Lee et al. (2004), who found that in the presence of mechanical vibration, CHF increased up to 12.6%. An accurate correlation was proposed for the CHF as a function of vibration

frequency and amplitude. Visual characterization of bubble nucleation and growth on the surface of a hot vibrating cylinder was undertaken by Atashi et al. (2014). They showed that vibration activates a new nucleation site on a hot surface and produces more bubbles with smaller sizes in comparison to the stationary condition of a solid surface. Therefore, bubbles more frequently detached from the surface, and a significant increase in the heat transfer coefficient was achieved.

More recently, Alangar (2017) investigated pool boiling on a flat test surface heated by a heater rode, which was mounted on a controllable vibration exciter. It was shown that the presence of mechanical vibration shifts the pool boiling curve toward lower wall superheats. This observation was the direct result of a heat transfer enhancement on a vibrating surface. Moreover, the heat transfer enhancement intensified with a frequency of vibration of up to 10 Hz. At higher frequencies, a decreasing/increasing trend was reported for the heat transfer enhancement ratio depending on the value of the surface heat flux and vibration amplitude.

The aforementioned experimental studies confirm the enhancing effect of mechanical vibration on pool boiling heat transfer on simple geometries, including flat surfaces and a single circular tube. However, for mechanical vibrations to be used as a reliable method for the enhancement of pool boiling heat transfer in a real heat exchanger, such techniques need to be evaluated by using more complex and practical geometries (e.g. tube arrays and tube bundles). For this purpose, numerical modelling can be used as an effective tool to provide us with detailed information on the temporal evolution of the flow and temperature fields of pool boiling in the presence of solid surface vibrations. Moreover, numerical simulations can be used to obtain more concise conclusions regarding the effects of various relevant parameters on pool boiling heat transfer to achieve the highest possible enhancement.

Numerical simulations were previously used to study the effects of vibration on a single-phase heat transfer (Shokouhmand and Abadi, 2010a, b; Shokouhmand et al., 2011; Vadasz et al., 2014). However, to the best of our knowledge, no attempt has been made thus far to tackle the two-phase pool boiling phenomenon over a vibrating solid surface using a numerical method.

Therefore, in this work, we intended to numerically simulate pool boiling on a vibrating array of vertically aligned circular tubes. Water at atmospheric conditions was selected as the boiling liquid, and a detailed survey on the effects of the vibration frequency and amplitude on the two-phase heat transfer was undertaken. The remainder of this manuscript is organized as follows: In sections 2 and 3, the governing equations of the pool boiling problem and the adapted numerical method are outlined, followed by a description of the numerical results obtained. Finally, the paper concludes with highlights describing the major findings.

2. Mathematical formulation

2.1. Problem description

To examine the effects of mechanical vibration on pool boiling heat transfer, a vertical array of five circular tubes with a diameter of D = 19 mm and length of L = 0.4 m is considered. The array pitch is denoted by S, and the vertical array is placed at the centre of an open rectangular container with a size of 0.8 m × 0.4 m. The container is filled with water at atmospheric pressure and its corresponding saturation temperature, and the tubes are heated uniformly with an adjustable heat flux of q''. As a result, boiling occurs on the surface of the heated tubes, and all tubes are simultaneously vibrated horizontally by an external exciter with a periodic velocity of $U = U_m Cos(2\pi ft)$, where t is time, U_m is the amplitude of the velocity

oscillation, and *f* is its frequency. A schematic of the assumed physical domain of our problem is depicted in Fig. 1.

2.2. Governing equations

During the course of pool boiling, the periodic nucleation and detachment of vapour bubbles from solid surfaces are accompanied by a natural circulation of the surrounding boiling liquid toward the heated surface. To resolve this two-phase flow field, in the present work, a multifluid formulation is adapted in which two sets of separate but interconnected conservation laws are solved for both the liquid and vapour phases. For a particular phase '*k*', conservation laws for the mass, momentum, and energy are given as follows (Drew, 1983) (ρ is the fluid density, *P* is the pressure, *u* is the velocity vector, *T* is the temperature, and *i* is the specific enthalpy):

$$\frac{\partial}{\partial t}\left(\alpha^k\rho^k\right)+\nabla.\left(\alpha^k\rho^k\boldsymbol{u}^k\right)=\sum_{l=1}^{N_P}\left(\dot{m}''^{lk}-\dot{m}''^{kl}\right) \tag{1a}$$

$$\begin{aligned}\frac{\partial}{\partial t}\left(\alpha^k\rho^k\boldsymbol{u}^k\right)+\nabla.\left(\alpha^k\rho^k\boldsymbol{u}^k\otimes\boldsymbol{u}^k\right)=\nabla.\left\{\alpha^k\left(\mu^k+\mu_T^k\right)\left[\nabla\boldsymbol{u}^k+\left(\nabla\boldsymbol{u}^k\right)^T-\frac{2}{3}I\left(\nabla.\boldsymbol{u}^k\right)\right]-\frac{2}{3}I\alpha^k k^k\right\}\\ -\alpha^k\nabla P+\alpha^k\rho^k\boldsymbol{g}+\sum_{l=1}^{N_P}\left(\dot{m}''^{lk}\boldsymbol{u}^l-\dot{m}''^{kl}\boldsymbol{u}^k\right)\\ +\boldsymbol{F}^{k,drag}+\boldsymbol{F}^{k,lift}+\boldsymbol{F}^{k,wall}+\boldsymbol{F}^{k,vm}+\boldsymbol{F}^{k,dispersion}\end{aligned} \tag{1b}$$

$$\begin{aligned}\frac{\partial}{\partial t}\left(\alpha^k\rho^k i^k\right)+\nabla.\left(\alpha^k\rho^k\boldsymbol{u}^k i^k\right)=\alpha^k\frac{\partial P}{\partial t}+\nabla.\left(\alpha^k\lambda^k\nabla T^k\right)+\nabla.\left(\alpha^k\frac{\mu_T^k}{Pr_T^k}\nabla i^k\right)\\ +\sum_{l=1}^{N_P}\left(\dot{m}''^{lk}i^l-\dot{m}''^{kl}i^k\right)+\sum_l h^{kl}\left(T^k-T^l\right)\end{aligned} \tag{1c}$$

where α^k is the volume fraction of the *k*-th phase, $\boldsymbol{g}$ is the gravitational acceleration, $\dot{m}''^{kl}$ is the mass flux transferred from the *k*-th phase to the *l*-th phase ($\dot{m}''^{kk}=0$), N_p is the number of

phases, λ^k is the thermal conductivity, h is the convection heat transfer coefficient between phases, and $\boldsymbol{F^k}$ is the resultant momentum interphase transfer force vector. Moreover, μ is the dynamic viscosity of the fluid, $\boldsymbol{\mu_T^k}$ is the turbulent viscosity computed using the realisable k-ε turbulence model (Avetissian et al., 2005), and Pr_T^k is the turbulent Prandtl number. In the k-ε turbulence model, a separate set of differential equations is solved for the turbulent kinetic energy (k^k) and turbulent dispersion (ε^k) of each phase, as follows:

$$\frac{\partial(\alpha^k\rho^k k^k)}{\partial t}+\nabla.\left(\alpha^k\rho^k k^k\boldsymbol{u}^k\right)=\nabla.\left(\alpha^k\frac{\mu_T^k}{\sigma_k}\nabla k^k\right)+\alpha^k\boldsymbol{\tau}_T^k:\boldsymbol{u}^k-\alpha^k\rho^k\varepsilon^k+S_{k^k}^{int} \tag{2a}$$

$$\frac{\partial(\alpha^k\rho^k\varepsilon^k)}{\partial t}+\nabla.\left(\alpha^k\rho^k\varepsilon^k\boldsymbol{u}^k\right)=\nabla.\left(\alpha^k\frac{\mu_T^k}{\sigma_\varepsilon}\nabla\varepsilon^k\right)+\alpha^k\frac{\varepsilon^k}{k^k}\left(C_{\varepsilon 1}\boldsymbol{\tau}_T^k:\nabla\boldsymbol{u}^k-C_{\varepsilon 2}\rho^k\varepsilon^k\right)+S_{\varepsilon^k}^{int} \tag{2b}$$

$$C_\mu=0.09,\quad \sigma_k=1.0,\quad \sigma_\varepsilon=1.3,\quad C_{\varepsilon 1}=1.44,\quad C_{\varepsilon 2}=1.92 \tag{2c}$$

$$S_{k^k}^{int}=-(\boldsymbol{F}^{k,drag}+\boldsymbol{F}^{k,vm}).(\boldsymbol{u}^l-\boldsymbol{u}^k) \tag{2d}$$

$$S_{\varepsilon^k}^{int}=C_{\varepsilon 3}\frac{S_{k^k}^{int}}{\tau_b},\ \tau_b=\frac{k^k}{\varepsilon^k} \tag{2e}$$

where $C_{\varepsilon 3}$ is equal to unity (Avetissian et al., 2005).

It should be noted that in all convection terms, the parameter u is the absolute fluid velocity vector, which is defined as the difference between the fluid and grid velocities ($u-\hat{u}$). The term $\hat{u}$ is the grid velocity. The grid motion is linearly distributed from the tube surface to the surrounding fluid. This method was successfully utilized in the previous works of (Shokouhmand and Abadi, 2010b; Shokouhmand et al., 2011).

The direct interphase heat transfer coefficient h^{kl} is calculated as follows based on the correlation of Ranz and Marshall (1952) for the Nusselt number in turbulent bubbly flows:

$$Nu^k = 2.0 + 0.15\, Re^{0.8}\, Pr^{0.5} \tag{3}$$

where *Re* and *Pr* are the Reynolds and Prandtl numbers, respectively.

A mechanistic model is used to estimate the mass transfer rate from the liquid phase of (*l*) to the gaseous phase of (*v*) during a boiling phase change, as follows (Lee, 1979):

$$\dot{m}''^{lv} = C_{MT}\, \alpha^l \rho^l \frac{T^l - T_{sat}}{T^v};\; C_{MT} = \frac{6}{d^v}\sqrt{\frac{M}{2\pi R T_{sat}}}\, i^{lv}\left(\frac{\alpha^v \rho^v}{\rho^v - \rho^l}\right) \tag{4}$$

where T_{sat} is the saturation temperature at the gas/liquid interface, R is the gas constant, M is the gas molecular weight, and i^{lv} is the latent heat of evaporation.

The drag force ($\boldsymbol{F}^{k,drag}$) between the liquid and gaseous phases is proportional to the velocity slip between liquid water and vapour bubbles, as presented in Eq. (5):

$$\boldsymbol{F}^{k,drag} = \frac{1}{8} C_D\, a_{if}\, \rho^k \left|\boldsymbol{u}^l - \boldsymbol{u}^k\right|\left(\boldsymbol{u}^l - \boldsymbol{u}^k\right) \tag{5}$$

where a_{if} is the interfacial area concentration and C_D is the drag coefficient, calculated from the correlation proposed by Clift et al. (1978) as

$$C_D = max\left[min\left(C_{D,ellipse}, C_{D,cap}\right), C_{D_{Sphere}} \right]$$

$$C_{D_{Sphere}} = \begin{cases} \dfrac{24}{Re} & Re \le 0.01 \\ 24\dfrac{\left(1+0.15\,Re^{0.687}\right)}{Re} & Re > 0.01 \end{cases}; \; C_{D,cap} = \frac{8}{3}; C_{D,ellipse} = \frac{4}{3}\frac{gd^l}{U_t^2}\frac{\left(\rho^k - \rho^l\right)}{\rho^l} \tag{6a}$$

$$Re = \frac{\rho^k \left|u^l - u^k\right| d^l}{\mu^k}; \; U_t = \frac{\mu^k}{\rho^k d^l} Mo^{-0.149}\left(J - 0.857\right); \; Mo = \frac{\left(\mu^k\right)^4 g\left(\rho^k - \rho^l\right)}{\left(\rho^k\right)^2 \sigma^3}$$

$$J = \begin{cases} 0.94H^{0.757} & 2 < H \le 59.3 \\ 3.42H^{0.441} & H > 59.3 \end{cases}; \; H = \frac{4}{3} Eo\, Mo^{-0.149}\left(\frac{\mu^k}{0.0009}\right)^{-0.14} \tag{6b}$$

$$Eo = \frac{g\left(\rho^k - \rho^l\right)\left(d^l\right)^2}{\sigma}$$

where Mo is the Morton number, Eo is the Eotvos number, σ is the surface tension, and d is the bubble diameter. The wall repulsive force ($\boldsymbol{F}^{k,wall}$) on the vapour bubbles, given by Antal et al. (1991), is

$$\boldsymbol{F}^{k,wall} = C_w \rho^k \alpha^l \left|\boldsymbol{u}^l - \boldsymbol{u}^k\right|^2 \boldsymbol{n}_w$$

$$C_w = max\left(0, \frac{C_{w1}}{d^l} + \frac{C_{w2}}{y_w}\right); \; C_{w1} = -0.01; \; C_{w2} = 0.05 \tag{7}$$

The virtual mass force originates from the acceleration of gas bubbles relative to the continuous liquid phase and can be calculated as

$$\boldsymbol{F}^{k,vm} = -\boldsymbol{F}^{l,vm} = 0.5\alpha^l \rho^k \left(\frac{D\boldsymbol{u}^l}{Dt} - \frac{D\boldsymbol{u}^k}{Dt}\right) \tag{8}$$

To account for the turbulent dispersion force, the formulation proposed by Burns et al. (2004) is employed:

$$\boldsymbol{F}^{k,dispersion} = -\boldsymbol{F}^{l,dispersion} = C_D \frac{\mu_T^l}{\rho^l Sc_b}\left(\frac{\nabla \alpha^l}{\alpha^l} - \frac{\nabla \alpha^k}{\alpha^k}\right) \tag{9}$$

where Sc is the Schmidt number. Finally, the lift force $\boldsymbol{F}^{k,lift}$ is approximated using the Tomiyama (1998) model, as shown in Eq. (10):

$$\boldsymbol{F}^{k,lift} = -\boldsymbol{F}^{l,lift} = C_L \alpha^l \rho^k \left(u^l - u^k\right) \times \left(\nabla \times u^k\right) \tag{10a}$$

$$C_L = \begin{cases} min\left[0.288 tanh\left(0.121 Re\right), f\left(Eo_d\right)\right] & Eo < 4 \\ f\left(Eo_d\right) = 0.00105 Eo_d{}^3 - 0.0159 Eo_d{}^2 - 0.0204 Eo_d + 0.474 & 4 < Eo < 10 \\ -0.29 & Eo > 10 \end{cases} \tag{10b}$$

$$Eo_d = \frac{g\left(\rho^k - \rho^l\right)\left(d^l\right)^2}{\sigma}\left(1 + 0.163 Eo^{0.757}\right)^{2/3}$$

2.3. RPI model for pool boiling

In the present work, the wall heat flux is computed using the robust RPI model (Kurul and Podowski, 1991), in which three components of the heat flux are accounted for during a liquid phase change on a solid surface: a single-phase convective heat flux between the solid surface and its surrounding fluid ($\dot{q}_C$), the latent heat flux of vaporization ($\dot{q}_E$), and the quenching flux owing to bubble departure from the surface ($\dot{q}_Q$). In the RPI model, the densities of the nucleation sites located on a solid surface are approximated using the

following power-law correlation (T_w is the wall temperature, and T_{sat} is the saturation temperature):

$$N_w = C^n \left(T_w - T_{sat}\right)^n ;\ C=210,\ n=1.805 \tag{11}$$

Single-phase convective heat transfer between heated surfaces and their surrounding fluid is given based on Newton's law of cooling as follows:

$$\dot{q}_C = h_C \left(T_w - T^l\right)\left(1 - A_b\right) \tag{12}$$

where h_C is the single-phase convective heat transfer coefficient, and A_b is the portion of a solid surface occupied by vapour bubbles calculated according to Eq. (13) (Del Valle and Kenning, 1985).

$$\begin{aligned} A_b &= min\left(1, K_{DK}\frac{N_W \pi D_W^2}{4}\right);\ K_{DK} = 4.8\, exp\left(-\frac{1}{80}\frac{\rho^l C_{p,l}\left(T_w - T^l\right)}{\rho^v i^{lv}}\right) \\ D_W &= min\left(0.0014, 0.0006\, exp\left(-\frac{\Delta T_W}{45}\right)\right) \end{aligned} \tag{13}$$

where D_w is the bubble departure diameter. The evaporative heat flux is proportional to the mass of nucleated bubbles, and can be approximated using the nucleation site density, i.e.

$$\dot{q}_E = \frac{\pi}{6} D_W^3 N_W \rho^v i^{lv} \tag{14}$$

Subsequently, the generated vapour mass at the solid $\left(\dot{m}''^{lv}\right)_w$ wall can be easily correlated as

$$\left(\dot{m}''^{lv}\right)_w = \frac{\dot{q}_E}{i^{lv} + C_{p,l}\left(T_{sat} - T^l\right)} \tag{15}$$

Finally, $\dot{q}_Q$ is related to the effective temperature gradient using Cole's model (Cole, 1960) for the bubble departure period (τ), as follows:

$$\dot{q}_Q = \frac{k^l}{\sqrt{\pi \frac{k^l}{\rho^l C_{p,l}} \tau}}\left(T_w - T^l\right); \frac{1}{\tau} = \sqrt{\frac{4g\left(\rho^l - \rho^v\right)}{3\rho^l D_w}} \tag{16}$$

3. Numerical method

3.1. Flow solver

The governing equations of pool boiling presented in Eq. (1) are numerically solved using the fully coupled flow solver available in the ANSYS FLUENT 17.1 CFD package. A second-order spatial and temporal discretization is utilized, and convective heat fluxes are approximated by a second-order upwind scheme. Transient simulations are conducted using a time step of 10^{-4} s, and the global convergence criterion is set at 10^{-6}.

Furthermore, the following assumptions are considered for the simulations:

1. The flow field is three-dimensional, transient, and turbulent.
2. The properties of each phase are assumed to be constant under the specified operating conditions.
3. The interface temperature is assumed to be at the saturation temperature.

4. A no-slip condition is considered for all walls within the computational domain.
5. The simulations continue until the changes in the pool boiling heat transfer coefficients reach below 2%. The corresponding time for this criterion is t = 20 s for all cases.
6. At the beginning of the simulation, the flow field is quiescent at a temperature of 373.15 ºC.
7. Pool opening: The upper part of the pool is open to attain saturation pressure.

3.2. Mesh size study

In the present work, an unstructured grid of triangular elements is used to discretize the flow domain. The optimum cell count is obtained from a detailed mesh size study. As an example from this study in Fig. 2, the average heat transfer coefficient on the tube surfaces is depicted for three different cell counts in the absence of mechanical vibration. As can be seen, using a numerical mesh with 529,774 control volumes is a good compromise between accuracy and computational cost. This numerical grid is used throughout the manuscript to simulate our problem.

4. Results and discussion

In this section, numerical results regarding the pool boiling heat transfer from a vibrating array of heated tubes are provided. Subsequent to the code verification, a detailed parametric study is presented to delineate the effects of vibration frequency, vibration amplitude, tube spacing, and heat flux on the pool boiling heat transfer rate. Finally, the heat transfer enhancing effect from mechanical vibration is thoroughly addressed.

4.1. Validation of numerical method

Kang (2016) conducted a series of well-designed experiments on pool boiling heat transfer from a vertical array of two circular tubes at several different inclination angles. To assure readers regarding the accuracy of the adapted numerical method, we attempted to simulate Kang's experiment for horizontal case using water at atmospheric pressure through the numerical method outlined in section 3. In Fig. 3, the numerical results are compared with the experimental boiling curve for the upper tube and the average heat transfer coefficient. A favourable agreement is shown between the numerical results and the experimental data, thereby confirming the reliability of our numerical method.

In Fig. 4 shows another validation case for a vibrating circular rod immersed in a pool of saturated water at atmospheric pressure (Alangar, 2017). The rod is vibrated vertically at the frequency of 2 Hz, and amplitudes of 1 or 2 mm. Further details about the experimental conditions and setup can be found in Alangar (2017). As can be seen in Fig. 4 the performance of the present numerical model is acceptable for predicting the effect of vibration on the pool boiling phenomenon.

4.2. Applicable ranges of parameters

In order to select the appropriate ranges of the governing parameters such as amplitude and frequency of vibration, distance between tubes, and heat flux for the simulations, an assessment of each parameter on the overall effect of the vibration on the boiling heat transfer coefficient was performed. This assessment is necessary to obtain the suitable ranges of the parameters that can be applicable for real use. The main purpose of this study is to find the optimum range to enhance the pool boiling heat transfer coefficient. Therefore, a parameter called the Enhancement Ratio (*ER*) is defined as a reliable measure of the two-phase heat transfer enhancement acquired by the vibration of a boiling surface, i.e.

$$ER(\%) = \frac{\left(\overline{HTC_{av}}\right)_{vib} - \left(HTC_{av}\right)_{no,vib}}{\left(HTC_{av}\right)_{no,vib}}, \tag{17}$$

where $\left(\overline{HTC_{av}}\right)_{vib}$ is the surface- and time-averaged heat transfer coefficient in the presence of vibrations computed over a sampling period of 20 s, and $(HTC_{av})_{no,vib}$ is the surface-averaged HTC for a stationary tube array.

Table 1 presents an assessment of results for different operating conditions. It can be seen that the higher the magnitude of vibration and heat flux, the more enhancement can be achieved. Therefore, there is no specific limit for this parameter. However, for cases of q'' > 20000 kW/m^2, the increase of the heat flux significantly diminishes the effect of oscillation. Therefore, q'' = 20000 kW/m^2 is chosen as the upper limit of the heat flux. The results for S/D show that an increasing S/D, particularly for the condition S/D > 4, has no considerable effect on the enhancement ratio. Therefore, S/D = 4 is the upper limit for S/D in this study. In fact, the heat transfer coefficient is not very sensitive to S/D. A similar conclusion was obtained in the previous works of Shokouhmand et al. (2011) regarding the natural convection. The most critical parameter is the frequency of vibration, which is claimed to have an optimum value by many authors depending on the geometry and operating conditions (Alangar, 2017; Atashi et al., 2014; Chou et al., 2002). In fact, the maximum applicable frequency depends on three major factors: the structural design of the heat transferring equipment, the available excess power needed for the generation of mechanical vibrations, and the degree of enhancement which is desirable for a certain application. The results show that an increase in the enhancement ratio for f > 2 is marginal. Therefore, in this study, only the effect of low-frequency oscillations on the nucleate pool boiling is considered. Based on

the above discussion, the ranges of various governing parameters are presented in Table 2. Furthermore, a thorough discussion of the heat transfer enhancement is given in section 4.6.

4.3. Overall effects of vibration

The effects of mechanical vibration on the contours of the vapour volume fraction are shown in Fig. 5. For a stationary tube array, large levels of void fraction are observed on the heated tube surfaces (particularly for the tubes located in the upper rows). This can be attributed to the formation of large vapour bubbles directly from the growth of nucleated bubbles on a solid surface, or to the coalescence of smaller bubbles. However when the tubes vibrate at a finite frequency, the level of vapour volume fraction decreases on the tube surface. Because mechanical vibration of a boiling surface forces the nucleated bubbles to detach more frequently from the solid surface and interrupts the growth of vapour bubbles, smaller vapour bubbles are generated and less of the flow domain is occupied by gaseous phases, particularly near the heated tubes. Moreover, this effect is intensified with an elevation of the vibration frequency, and for larger frequencies, smaller and more uniformly distributed vapour bubbles are present over the boiling surface.

The fluid temperature field during pool boiling is also affected by the mechanical vibrations of the boiling surface. As can be seen in Fig. 6, the wall temperature of the vibrating tubes is noticeably lower than that of the stationary tubes, particularly for lower rows within the array. This trend strongly confirms the enhancing effect of mechanical vibration on pool boiling heat transfer. To corroborate this deduction, time-averaged heat transfer coefficients of pool boiling for multiple vibration frequencies, presented in Fig. 7, are compared to the corresponding values for a stationary tube array. A significant increase in the HTC is reported for vibrating tube arrays, and the heat transfer rate increases as the vibration frequency

increases. Moreover, the temperature and HTC distribution are more uniform across the tube array when a vibration is present.

4.4. Effects of vibration frequency and amplitude

As shown in Fig. 8, after an initial transient response, the pool boiling HTC varies periodically over time at a frequency identical to the frequency of the tube array oscillation. This periodic evolution of the HTC is a direct result of the tube motion, which breaks the thermal boundary layer on the tube surface, generates a strong flow of boiling liquid, and enhances the convective portion of heat transfer from the boiling surface. Therefore, during a single period of tube vibration, when the tube velocity is high (within the vicinity of the equilibrium point), the HTC peaks accordingly, and by contrast, at the two end points, the HTC decreases when the tube moves toward zero velocity. Moreover, the amplitude of HTC oscillation decreases as the frequency of vibration increases. As the variations of the heat transfer coefficients for the upper tubes are very similar to each other, only the results for tube three are presented.

It is also interesting to examine the temperature distribution on the tube surfaces, as shown in Fig. 9. The temperature distribution on the tube surfaces is strongly affected by the natural circulation of a boiling liquid, bubble nucleation and detachment, and the force of liquid motion caused by a vibration of the tube surface. The combination of these three effects produces a rather complex temperature field on the tube surface. As can be seen, the maximum temperature occurs at a stagnation point of force fluid motion (θ = 90º and 270º), which is the direct result of a fierce suppression of bubble nucleation by the vibration-induced fluid motion.

Moreover, two local minima are reported in the temperature profile: one at the bottom of the tube (θ = 0º) where the free convection thermal boundary layer is extremely thin, and the other at the top (θ = 180º) of the tube where a considerable number of nucleation sites are present (see Fig. 5). The arrival of a detached vapour bubble from the lower tubes agitates the flow field around the upper tubes and increases the heat transfer rate. As a result, the wall temperature decreases across the tube array, and lower temperature levels are observed for tubes located in the upper rows (see Fig. 9c). In addition, increasing the vibration frequency reduces the minimum wall temperatures for all tubes within the array owing to a further enhancement in the pool boiling heat transfer rate from the vibrating boiling surfaces.

The effects of the vibration amplitude on the temporal evolution of the heat transfer coefficient for pool boiling are shown in Figs. 10 and 11. As can be observed, the amplitude of HTC oscillation increases when the tube vibration amplitude is elevated. Subsequently, the time-averaged heat transfer coefficient grows with the vibration amplitude**.** This stems from an increase in the velocity magnitude of the forced fluid motion prompted by the tube vibration. As a final note, it should be mentioned that as the amplitude of mechanical vibration increases, the thermal performances of the different tubes within the array begin to converge, and the spatial variation in the heat transfer rate across the height of the tube array decreases significantly (see Fig. 11).

4.5. Effects of heat flux and tube spacing

In this section, we investigate the effects of the heat flux magnitude and tube spacing on the pool boiling heat transfer from a vibrating tube array. As shown in Fig. 12, where the temporal evolution of the heat transfer coefficient from the first and last rows of the array are illustrated for three heat fluxes, the value of the heat transfer coefficient increases with an

increase in the heat flux. However, no clear alteration is observed in the functional form of HTC variation with time when the heat flux is increased. Moreover, a slight decrease in the amplitude of the HTC oscillation is shown with an increase in the heat flux.

It is also important to examine the effects of the heat flux on the temperature distribution on the tube surfaces, as shown in Fig. 13. The variations of the temperature for the upper tubes are very similar to each other; therefore, only the results for tube three are presented. As can be seen, the temperature increases almost uniformly on the tube surface when the heat flux is elevated. Additionally, the locations of the maximum and minimum temperatures on the tube surface nearly coincide for the various heat fluxes considered in the present work. The pitch-to-diameter ratio of (S/D) is the most important geometric parameter for an array of circular tubes, and subsequently its effects on the temperature field and heat transfer rate are shown in Figs. 14-16. As can be seen, the effects of the pitch-to-diameter ratio are negligible on the temporal variation of the HTC (Fig. 14). The trends for the variations in the circumferential tube surface temperature (Fig. 15) are similar for all values of S/D. The results show that the increasing the value of S/D has no effect on tube, as expected, but it causes some fluctuations on the surface temperature of the upper tubes due to the motion of the produced vapour to the upward direction. Finally, the vapour volume fraction decreases with (S/D) subsequent to the longer distances that the detached bubbles from the lower tubes need to travel in order to arrive at the surfaces of the upper tubes, as well as from the deaccelerating effect of the surrounding viscous liquid (Fig. 16).

4.6. Heat transfer enhancement

In Figs. 17 and 18, the contours of (ER) are illustrated as a function of the heat flux and vibration frequency for two vibration amplitudes. As can be seen, for all cases studied in the

present work the heat transfer increases when the boiling surface vibrates. Up to a 90% increase in the heat transfer rate is achieved through the vibration of a tube array. Moreover, the maximum value of *ER* increases with the amplitude of vibration, and this maximum value is located at the low-flux region of the pool boiling curve. As a result, the application of vibration to enhance the pool boiling heat transfer is most beneficial when the heat flux is moderately low.

4.7. Evolution of the flow field with time

In this section, the evolution of the flow field with time, presented as changes in the vapour volume fraction and liquid velocity, is explained to further investigate the effect of oscillations on the pool boiling phenomenon. Figs. 19 and 20 show the variations of the liquid z-velocity (Fig. 19) and vapour volume fraction (Fig. 20) along the centreline of the domain with time for f = 1 Hz, S/D = 3, q'' = 10 kW/m^2, and U_m = 0.2 m/s.

In Fig. 19, the variations of the liquid z-velocity are depicted. The results show that the liquid velocity increases as the time elapses. This can be attributed to two reasons: the pool boiling and corresponding buoyancy force, and the vibrations of the tube bundle. Fig. 19 also shows that at the vicinities of the tube surfaces owing to the effect of oscillations, the plots experience some partial maximum points. It should also be noticed that the z-velocity becomes zero at two stagnation points for each tube (bottom and top points). Another point is that the variations of the liquid z-velocity become stable for t > 20.

As can be seen in Fig. 20, the vapour volume fraction increases as the time advances. Similar to the plots for the liquid z-velocity, the vapour volume fraction profiles reach a stable condition at t > 20. In the vicinity of each tube owing to the formation of the vapour phase

from the tube surfaces, the vapour volume fraction suddenly increases. As a result, five peaks can be seen for each profile, which corresponds to a tube (as illustrated in Fig. 20). The vapour volume fraction decreases in the space between each tube because the produced vapour scatters to its surroundings as a result of tubes vibrations and buoyancy force.

5. Conclusion

A numerical simulation of pool boiling heat transfer from a vibrating array of circular tubes was addressed in the present work. For the liquid and vapour phases, a separate set of governing equations is solved numerically using the finite volume method on the ANSYS FLUENT 17.1 platform. To account for the heat removal by vapour bubble nucleation and detachment from a solid surface, the RPI boiling method is employed. The main conclusions of the present work can be summarized as follows:

i. For the entire range of relevant parameters considered in the present work, the pool boiling heat transfer intensifies in the presence of mechanical vibration.
ii. An increase of up to 90% in the heat transfer coefficient can be achieved through the vibrations caused by a forced fluid motion induced by surface boiling.
iii. The results showed that the increasing frequency of oscillation at more than 2 Hz does not affect the enhancement ratio significantly. Therefore, this value can be considered as the optimum value for the frequency of vibrations.
iv. The heat transfer rate increases with the frequency/amplitude of mechanical vibration.
v. The enhancing effect of vibration is most vigorous for moderately low heat fluxes.
vi. The pitch-to-diameter ratio has a negligible effect on the enhancing effect of a vibration.

References

Alangar, S., 2017. Effect of boiling surface vibration on heat transfer. Heat Mass Transf. 53, 73-79.

Antal, S.P., Lahey, R.T., Flaherty, J.E., 1991. Analysis of phase distribution in fully developed laminar bubbly two-phase flow. Int. J. of Multi. Flow 17, 635-652.

Atashi, H., Alaei, A., Kafshgari, M.H., Aeinehvand, R., Rahimi, S.K., 2014. New Pool Boiling Heat Transfer in the Presence of Low-Frequency Vibrations Into a Vertical Cylindrical Heat Source. Exp. Heat Transf. 27, 428-437.

Avetissian, A.R., Philippov, G.A., Zaichik, L.I., 2005. The effect of turbulence on spontaneously condensing wet-steam flow. Nuc. Eng. Des. 235, 1215-1223.

Bergles, A.E., 1969. The Influence of Heated-Surface Vibration on Pool Boiling. J. Heat Transf. 91, 152-154.

Burns, A.D., Frank, T., Hamill, I., Shi, J.M., 2004. The Favre averaged drag model for turbulent dispersion in Eulerian multi-phase flows. Fifth International Conference on Multiphase Flow, ICMF, Yokohama, Japan.

Chou, H.M., Horng, R.F., Liu, Y.S., 2002. The effects of vibration and reciprocating on boiling heat transfer in cylindrical container. Int. Commun. Heat Mass Transf. 29, 87-95.

Clift, R., Grace, J.R., Weber, M.E., 1978. Bubbles, drops and particles. Academic Press, New York.

Cole, R., 1960. A photographic study of pool boiling in the region of the critical heat flux. AIChE J. 6, 533-538.

Del Valle, V.H., Kenning, D.B.R., 1985. Subcooled flow boiling at high heat flux. Int. J. Heat Mass Transf. 28, 1907-1920.

Di Marco, P., Grassi, W., 2011. Effects of external electric field on pool boiling: Comparison of terrestrial and microgravity data in the ARIEL experiment. Exp. Therm. Fluid Sci. 35, 780-787.

Drew, D.A., 1983. Mathematical Modeling of Two-Phase Flow. Ann. Rev. Fluid Mech. 15, 261-291.

Gorgy, E., Eckels, S., 2012. Local heat transfer coefficient for pool boiling of R-134a and R-123 on smooth and enhanced tubes. Int. J. Heat Mass Transf. 55, 3021-3028.

Kang, M.G., 2016. Pool boiling heat transfer from an inclined tube bundle. Int. J. Heat Mass Transf. 101, 445-451.

Kim, D.E., Yu, D.I., Jerng, D.W., Kim, M.H., Ahn, H.S., 2015. Review of boiling heat transfer enhancement on micro/nanostructured surfaces. Exp. Therm. Fluid Sci. 66, 173-196.

Kurul, N., Podowski, M.Z., 1991. On the modelling of multidimensional effects in boiling channels, the 27th National Heat Transfer Conference, Minneapolis, USA.

Lee, W.H., 1979. A Pressure Iteration Scheme for Two-Phase Modeling. Technical Report LA-UR 79-975. Los Alamos Scientific Laboratory, Los Alamos, New Mexico.

Lee, Y.H., Kim, D.H., Chang, S.H., 2004. An experimental investigation on the critical heat flux enhancement by mechanical vibration in vertical round tube. Nuc. Eng. Des. 229, 47-58.

Markov, I.I., 1980. Boiling and condensation. Riga, 33-39.

Patil, C.M., Kandlikar, S.G., 2014. Review of the manufacturing techniques for porous surfaces used in enhanced pool boiling. Heat Trans. Eng. 10, 887-902.

Prinsnyakov, V.F., Navruzov, Y.V., Mamotov, P.V., Atoichev, A.V., 1992. Characteristics of heat emission from a vibrating heat High Temperature 30, 90-94.

Prisnyakov, V.F., Prisnyakov, K.V., 2001. Action of Vibrations on Heat and Mass Transfer in Boiling. J. Eng. Phys.Thermophys. 74, 1015-1023.

Ranz, W.E., Marshall, W.R., 1952. Vaporation from Drops, Part I. Chem. Eng. Prog. 48, 141-146.

Schaffrath, A., Hicken, E.F., Jaegers, H., Prasser, H.M., 1999. Operation conditions of the emergency condenser of the SWR1000. Nuc. Eng. Des. 188, 303-318.

Shoghl, S.N., bahrami, M., 2013. Experimental investigation on pool boiling heat transfer of ZnO, and CuO water-based nanofluids and effect of surfactant on heat transfer coefficient. Int. Commun. Heat Mass Transf. 45, 122-129.

Shokouhmand, H., Abadi, S.M.A.N.R., 2010a. The effect of Vertical vibrations on Natural Heat Transfer from an Isothermal Array of Cylinders. Comput. Sherm. Sci.: An Int. J. 2, 525-534.

Shokouhmand, H., Abadi, S.M.A.N.R., 2010b. Finite element analysis of natural heat transfer from an isothermal array of cylinders in presence of vertical oscillations. Heat Mass Transf. 46, 891-902.
Shokouhmand, H., Noori Rahim Abadi, S.M.A., Jafari, A., 2011. The effect of the horizontal vibrations on natural heat transfer from an isothermal array of cylinders. Int. J. Mech. Mater. Des. 7, 313.
Stutz, B., Morceli, C.H.S., da Silva, M.d.F., Cioulachtjian, S., Bonjour, J., 2011. Influence of nanoparticle surface coating on pool boiling. Exp. Therm. Fluid Sci. 35, 1239-1249.
Surtaev, A.S., S.Serdyukov, V., Pavlenko, A.N., 2016. Nanotechnologies for thermophysics: Heat transfer and crisis phenomena at boiling. Nanotechnologies in Russia 11, 696-715.
Sutharshan, B., Mutyala, M., Vijuk, R.P., Mishra, A., 2011. The AP1000TM Reactor: Passive Safety and Modular Design. Energy Proc. 7, 293-302.
Tomiyama, A., 1998. Struggle with computational bubble dynamics, Third International Conference on Multiphase Flow Lyon, France, 8-12 June.
Ustinov, A., Ustinov, V., Mitrovic, J., 2011. Pool boiling heat transfer of tandem tubes provided with the novel microstructures. Int. J. Heat Fluid Flow 32, 777-784.
Vadasz, J.J., Meyer, J.P., Govender, S., 2014. Chaotic and Periodic Natural Convection for Moderate and High Prandtl Numbers in a Porous Layer subject to Vibrations. Transport Porous Media 103, 279-294.
Vinko, Z., Naim, A., 1994. Boiling Heat Transfer From Oscillating Surface. 1, 191-196.

Figure captions

Figure 1. Computational domain with important measures.

Figure 2. Effect of grid size on heat transfer coefficient within stationary tube array for S/D = 2: (a) q'' = 5 kW/m^2 and (b) q'' = 60 kW/m^2.

Figure 3. Comparison between present numerical results and experiment results of Kang (2016): (a) heat transfer coefficient and (b) difference in wall temperature.

Figure 4. Comparison between the present numerical results and the experimental data of Alangar (2017) for the vibrating rod immersed in saturated water pool at atmospheric pressure.

Figure 5. Effects of mechanical vibration on vapour volume fraction for (a) f = 0, (b) f = 0.25, (c) f = 0.5, and (d) f = 1.0 (q'' = 10 kW/m^2, U_m = 0.2 m/s, S/D = 2).

Figure 6. Effects of mechanical vibration on temperature distribution (in Kelvin) for (a) f = 0, (b) f = 0.25, (c) f = 0.5, and (d) f = 1 (q'' = 10 kW/m^2, U_m = 0.2 m/s, S/D = 2).

Figure 7. Time-averaged heat transfer coefficient across vertical tube array (q'' = 10 kW/m^2, U_m = 0.2 m/s, S/D = 2).

Figure 8. Variations of heat transfer coefficient over time for tube 3 (q'' = 5 kW/m^2, U_m = 0.5 m/s, S/D = 4).

Figure 9. Circumferential tube wall temperature profiles at t = 20 s: (a) tube 1 for three frequencies, (b) tube 3 for three frequencies, and (c) tube array at f = 0.5 Hz (q'' = 5 kW/m^2, U_m = 0.2 m/s, S/D = 2).

Figure 10. Temporal variations of heat transfer coefficient: (a), (b) for two values of U_m at tube 1 and tube 5 (q'' = 20 kW/m^2, f = 0.5 Hz, S/D = 2), and (c), (d) for all tubes at U_m = 0.2 m/s and U_m = 0.5 m/s (q'' = 10 kW/m^2, f = 0.25 Hz, S/D = 4).

Figure 11. Time-averaged heat transfer coefficient along height of tube array for two vibration amplitudes (q'' = 20 kW/m^2, f = 0.5 Hz, S/D = 2).

Figure 12. Temporal evolution of heat transfer coefficient for different heat fluxes: (a), (b) tube 1 and tube 5 with (U_m = 0.2 m/s, f = 0.25 Hz, S/D = 2), (c), (d) tube 1 and tube 5 with (U_m = 0.5 m/s, f = 0.5 Hz, S/D = 4).

Figure 13. Circumferential tube wall temperature profiles at t = 20 s for different heat fluxes for tube 3 (U_m = 0.5 m/s, f = 0.5 Hz, S/D = 3).

Figure 14. Variations of heat transfer coefficient over time for different S/D values: (a) tube 1, (b) tube 3, and (c) tube 5 (q'' = 10 kW/m^2, U_m = 0.5 m/s, f = 0.25 Hz).

Figure 15. The effect of pitch-to-diameter ratio on circumferential tube wall temperature profiles at t = 20 s: (a) tube 1, (b) tube 3, and (c) tube 5 (q'' = 10 kW/m^2, Um = 0.25 m/s, f = 0.25 Hz)

Figure 16. Effect of pitch-to-diameter ratio on vapour volume fraction distribution for (a) S/D=2, (b) S/D=3, and (c) S/D=4 (q'' = 20 kW/m^2, U_m = 0.5 m/s, f = 1.0 Hz).

Figure 17. Heat transfer enhancement within tube array for U_m = 0.2 m/s.

Figure 18. Heat transfer enhancement within tube array for U_m = 0.5 m/s.

Figure 19. Variations of liquid z-velocity along centreline of domain during time for f = 1 Hz, S/D = 3, q'' = 10 kW/m^2, and U_m = 0.2 m/s.

Figure 20. Variations of vapour volume fraction along centreline of domain during time for f = 1 Hz, S/D = 3, q'' = 10 kW/m^2, and U_m = 0.2 m/s.

Table captions

Table 1. Enhancement of boiling heat transfer coefficient for different operating conditions.

Table 2. Range of variations in parameters considered in present study.

Figures

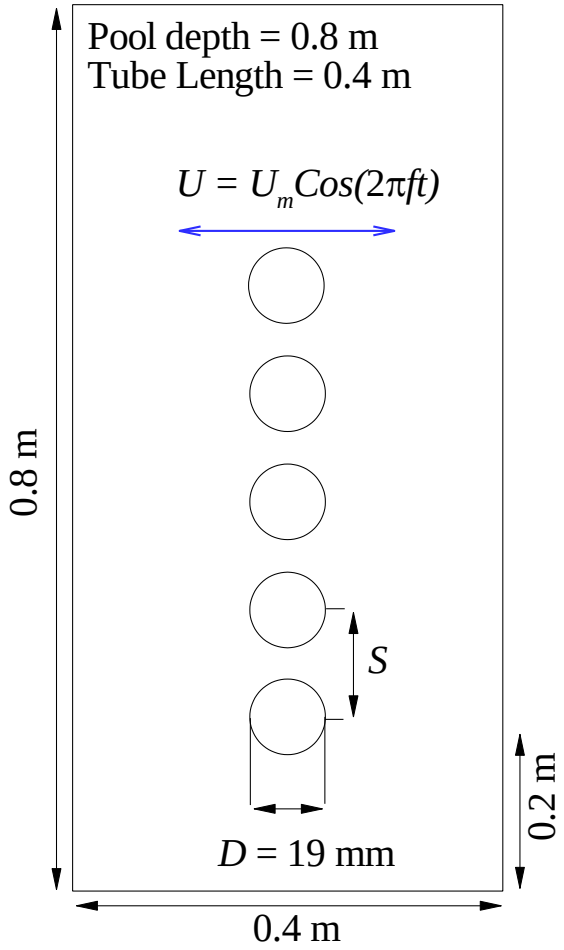

Figure 1

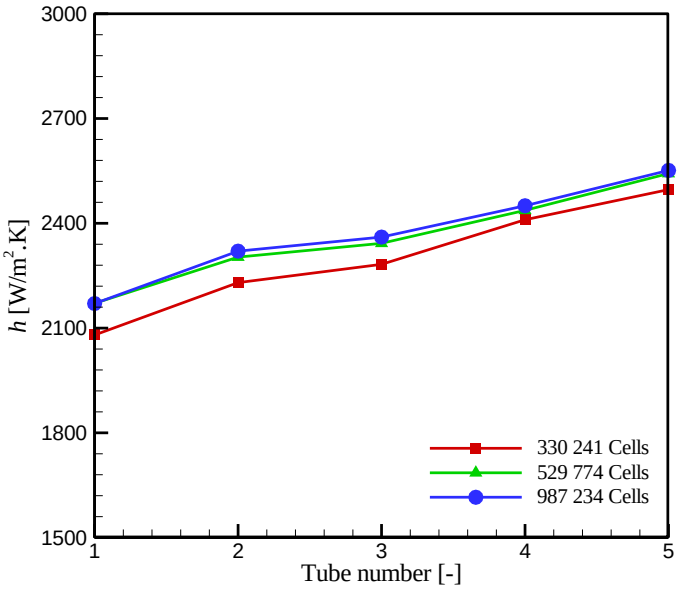
3000
2700
2400
2100
1800
1500
h [W/m².K]
1
2
3
4
5
Tube number [-]
330 241 Cells
529 774 Cells
987 234 Cells

(a)

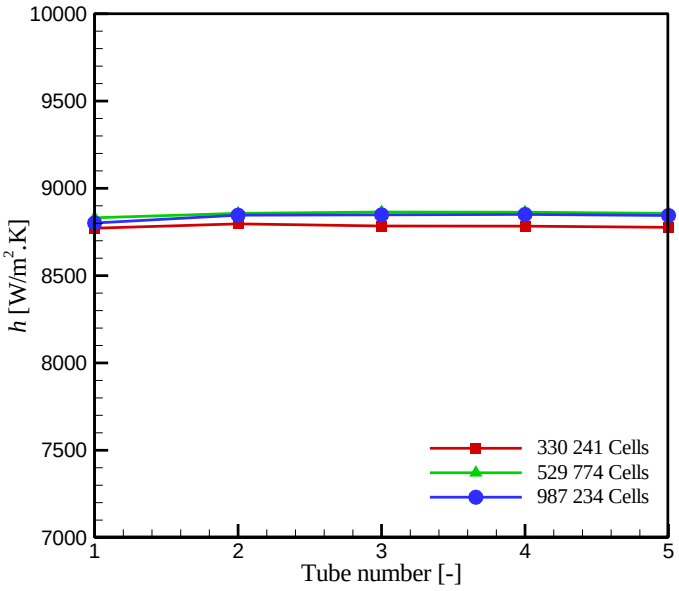
10000
9500
9000
8500
8000
7500
7000
h [W/m².K]
1
2
3
4
5
Tube number [-]
330 241 Cells
529 774 Cells
987 234 Cells

(b)

Figure 2

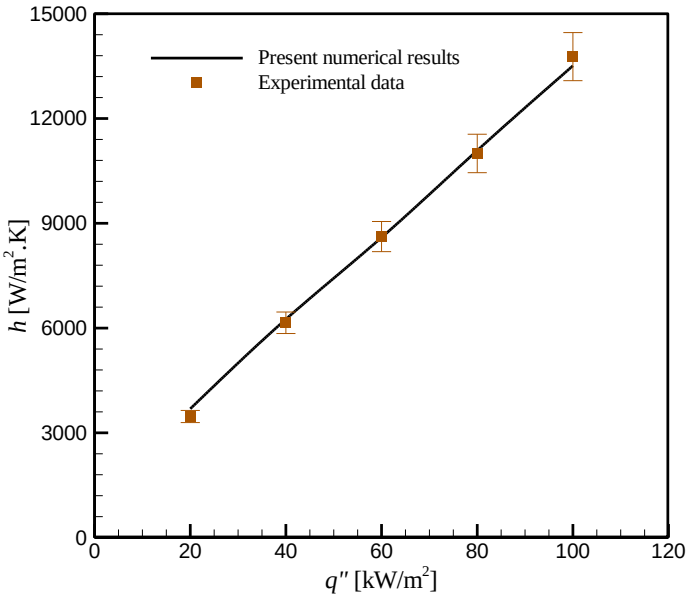
Present numerical results
Experimental data
h [W/m².K]
q″ [kW/m²]
0
3000
6000
9000
12000
15000
0
20
40
60
80
100
120

(a)

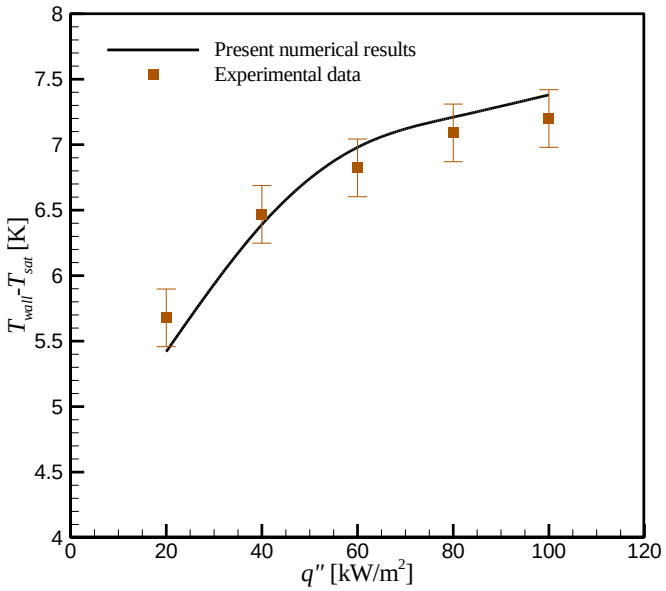
Present numerical results
Experimental data
T_wall-T_sat [K]
q″ [kW/m²]
4
4.5
5
5.5
6
6.5
7
7.5
8
0
20
40
60
80
100
120

(b)

Figure 3

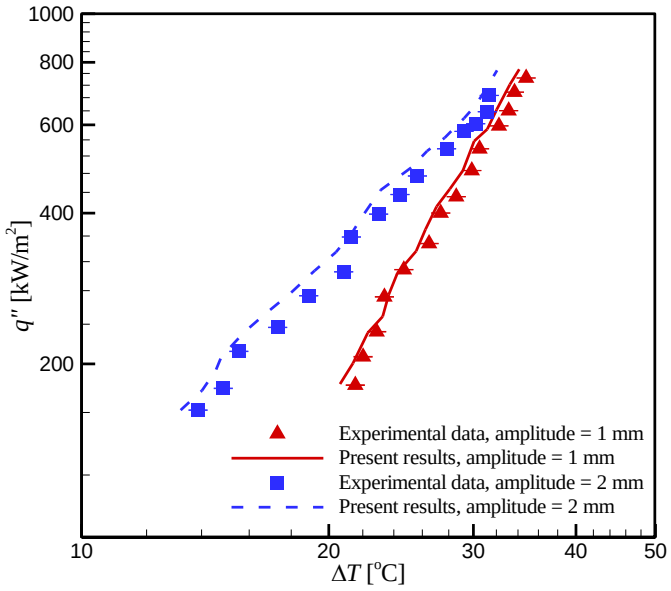
1000
800
600
400
200
q'' [kW/m2]
10
20
30
40
50
ΔT [°C]
Experimental data, amplitude = 1 mm
Present results, amplitude = 1 mm
Experimental data, amplitude = 2 mm
Present results, amplitude = 2 mm

Figure 4

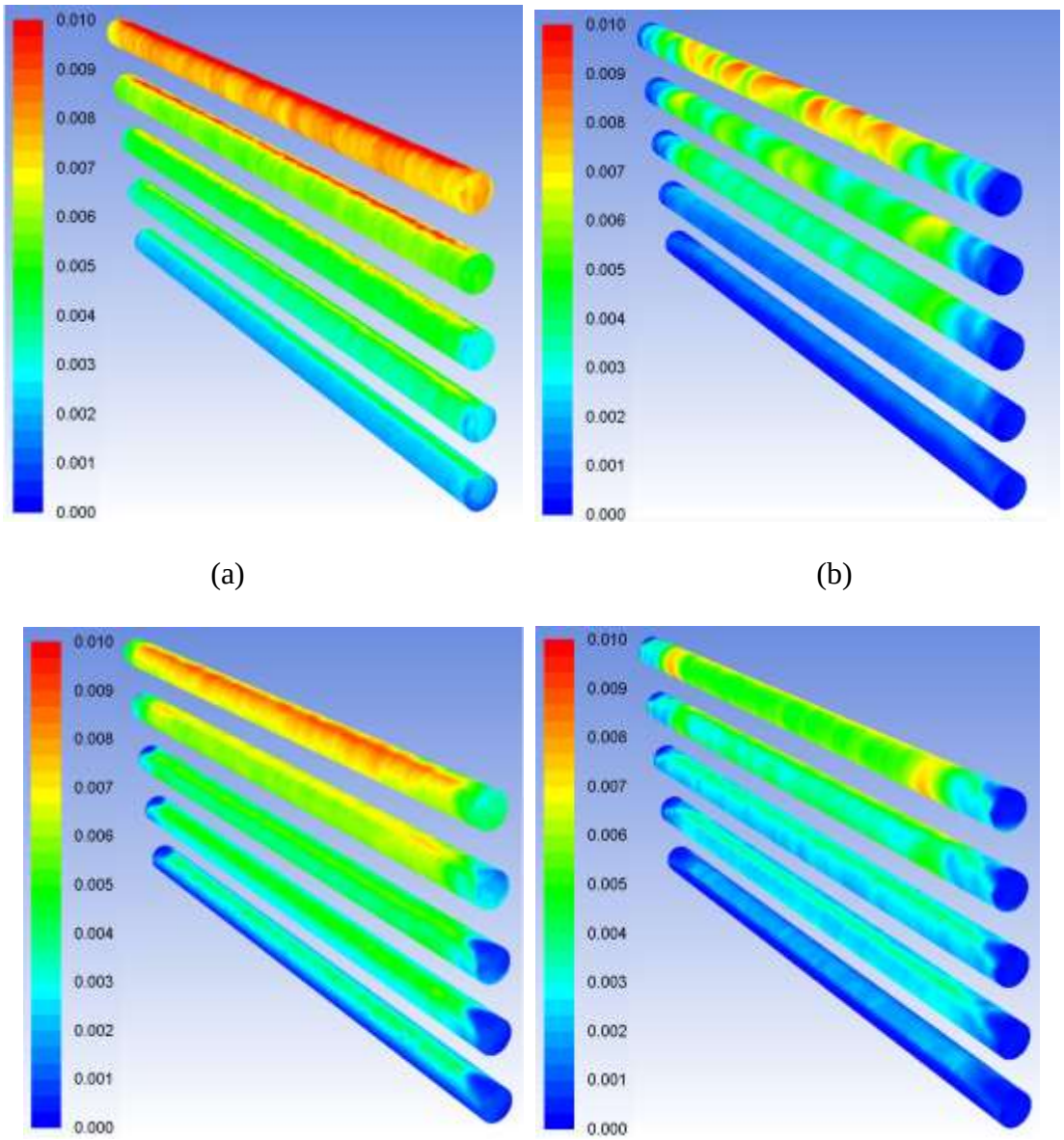

(a) (b)

(c) (d)

Figure 5

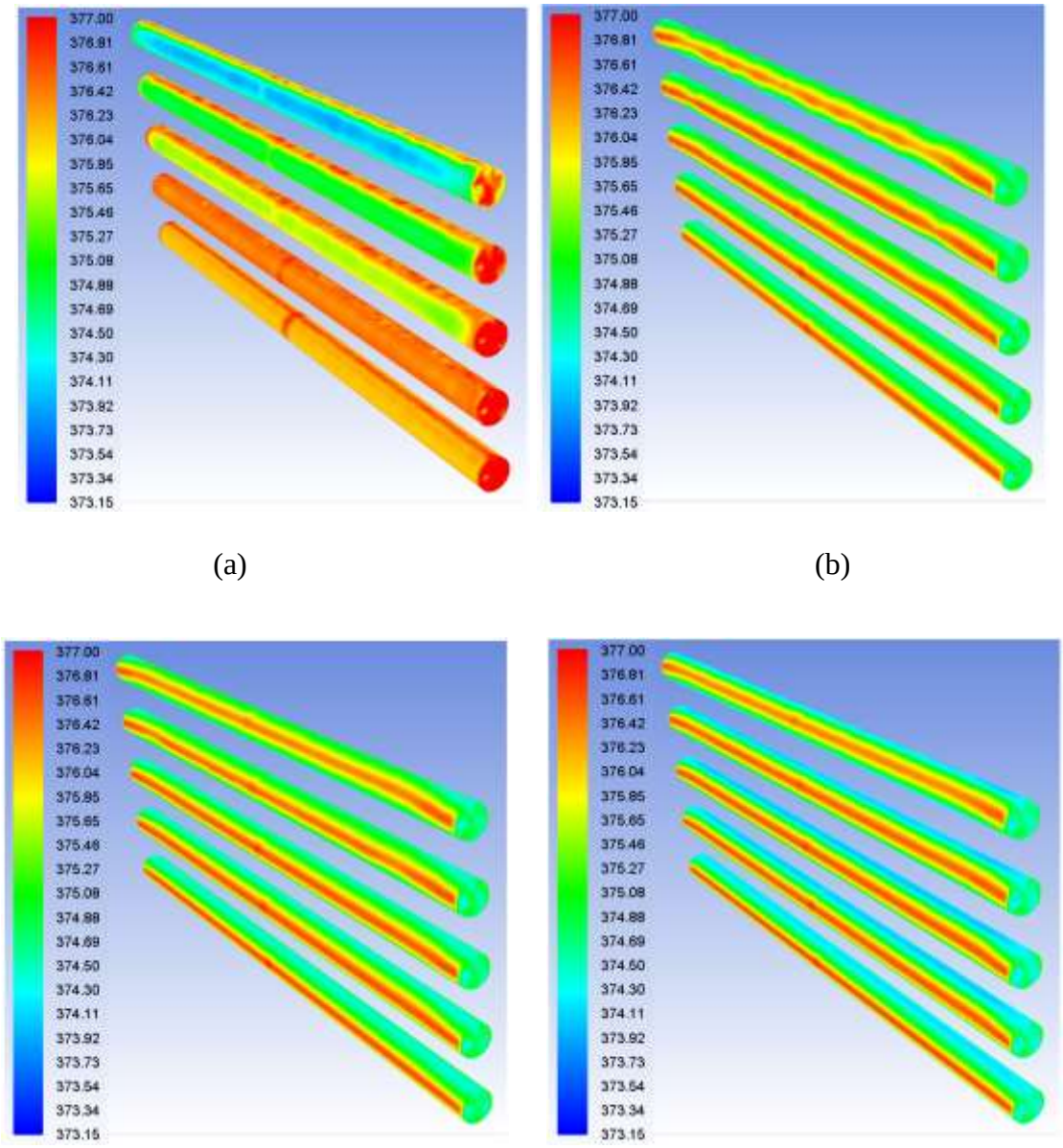
377.00
376.81
376.61
376.42
376.23
376.04
375.85
375.65
375.46
375.27
375.08
374.88
374.69
374.50
374.30
374.11
373.92
373.73
373.54
373.34
373.15
(a)
(b)
(c)
(d)

Figure 6

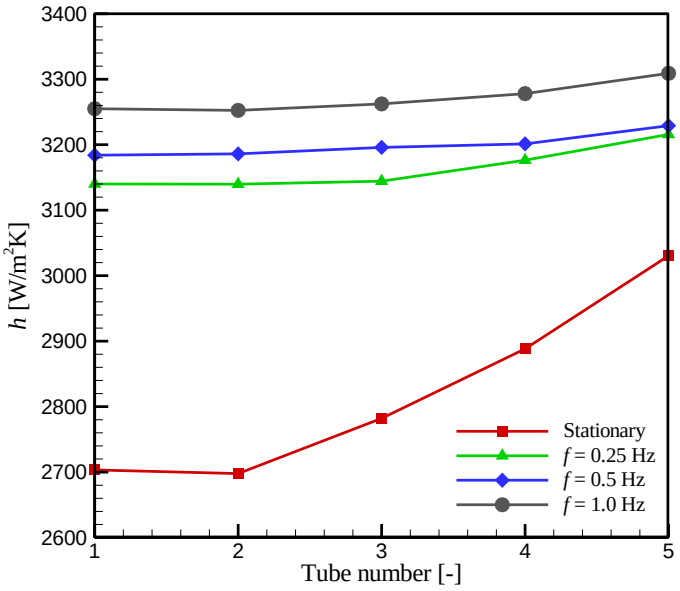
3400
3300
3200
3100
3000
2900
2800
2700
2600
h [W/m²K]
1
2
3
4
5
Tube number [-]
Stationary
f = 0.25 Hz
f = 0.5 Hz
f = 1.0 Hz

Figure 7

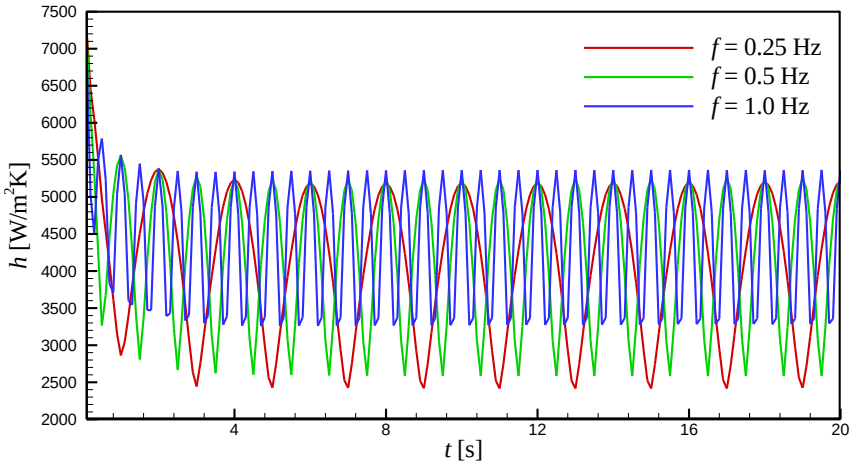
7500
7000
6500
6000
5500
5000
4500
4000
3500
3000
2500
2000
h [W/m²K]
4
8
12
16
20
t [s]
f = 0.25 Hz
f = 0.5 Hz
f = 1.0 Hz

Figure 8

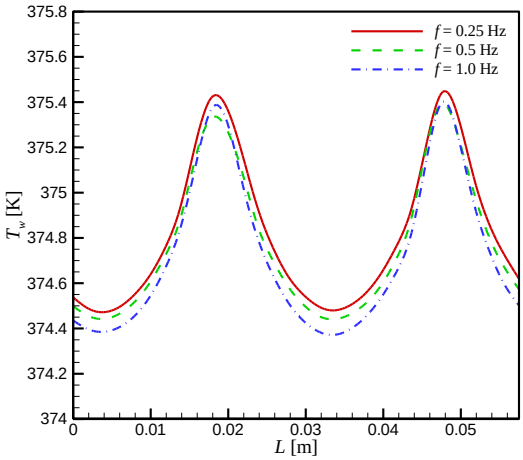
f = 0.25 Hz
f = 0.5 Hz
f = 1.0 Hz
T_w [K]
L [m]

(a)

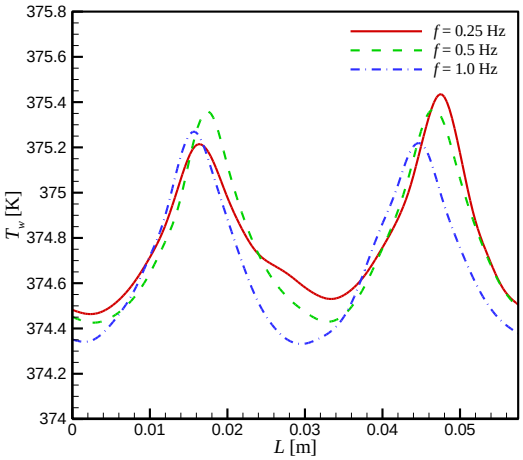
f = 0.25 Hz
f = 0.5 Hz
f = 1.0 Hz
T_w [K]
L [m]

(b)

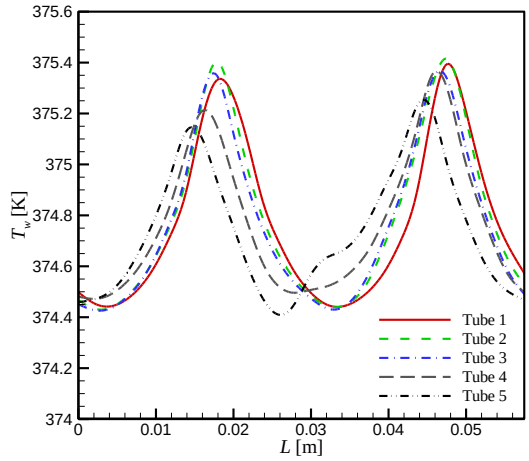
Tube 1
Tube 2
Tube 3
Tube 4
Tube 5
T_w [K]
L [m]

(c)

Figure 9

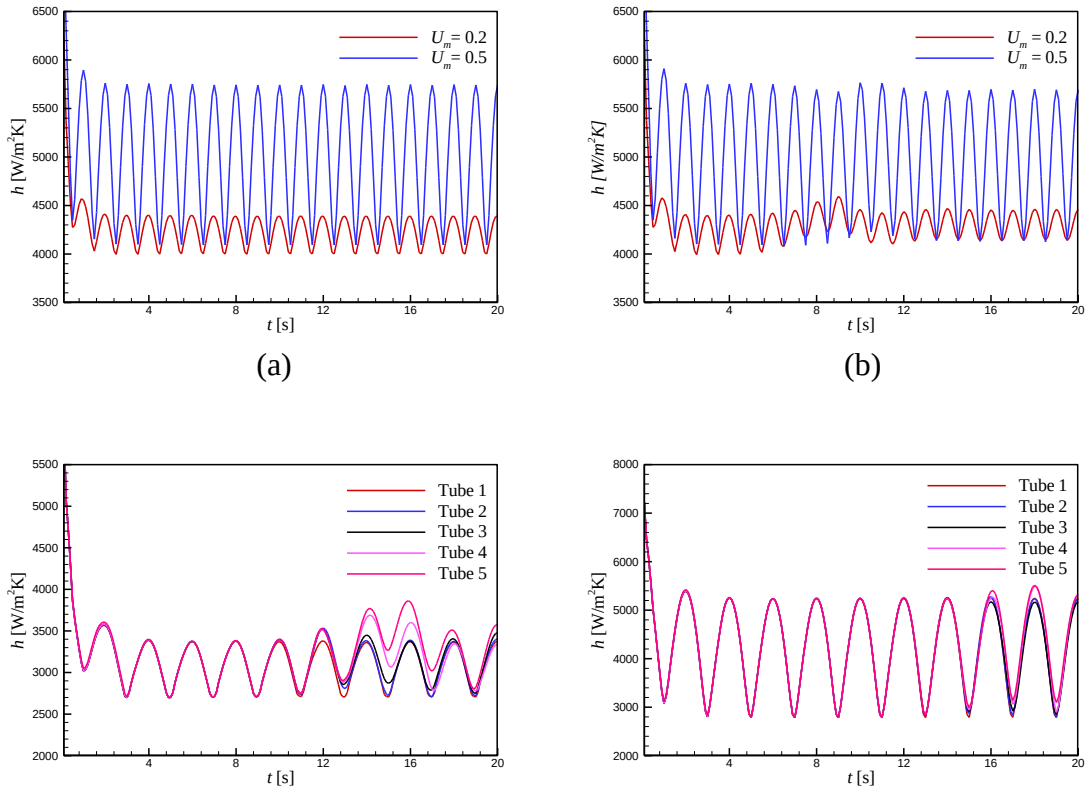

Figure 10

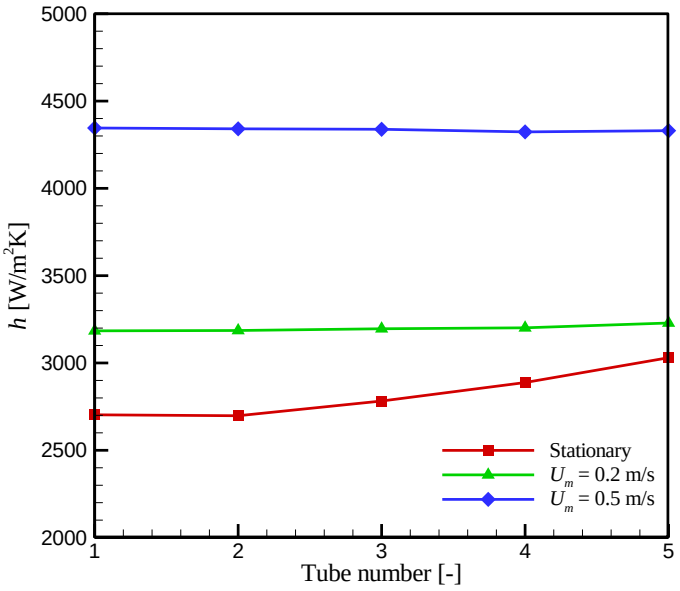
5000
4500
4000
3500
3000
2500
2000
h [W/m²K]
1
2
3
4
5
Tube number [-]
Stationary
U_m = 0.2 m/s
U_m = 0.5 m/s

Figure 11

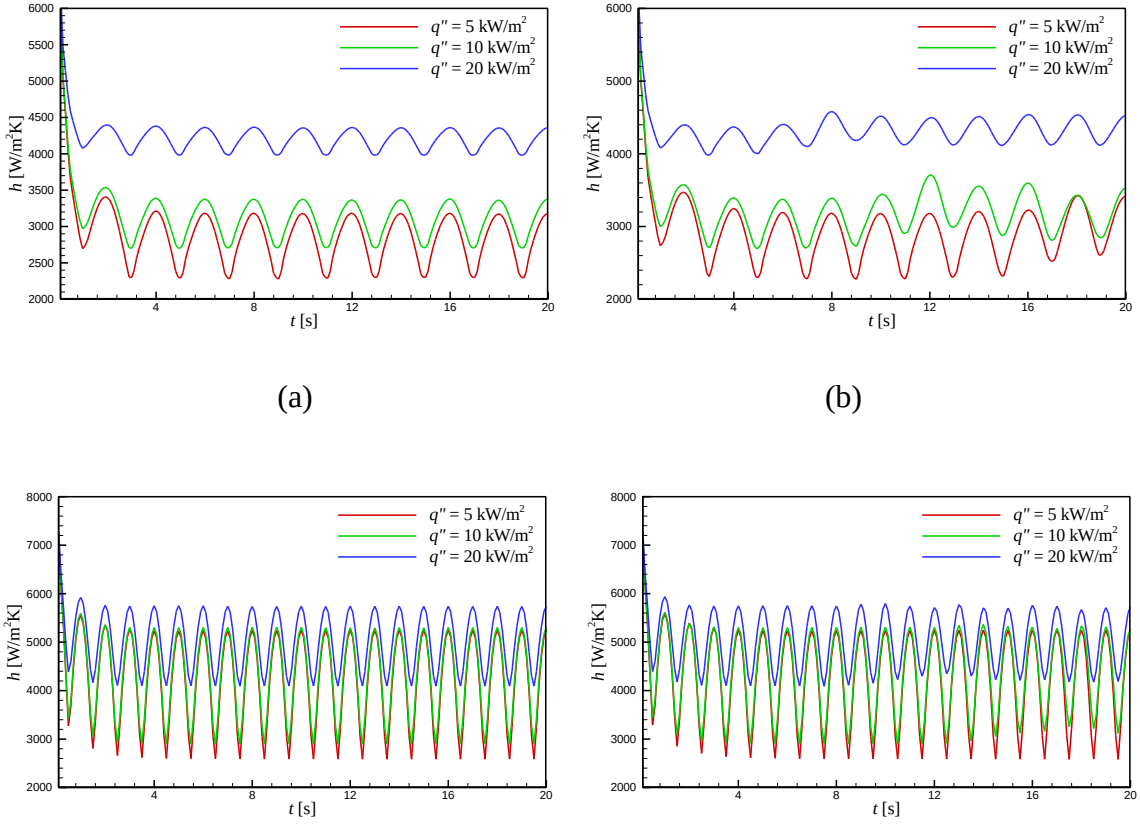

Figure 12

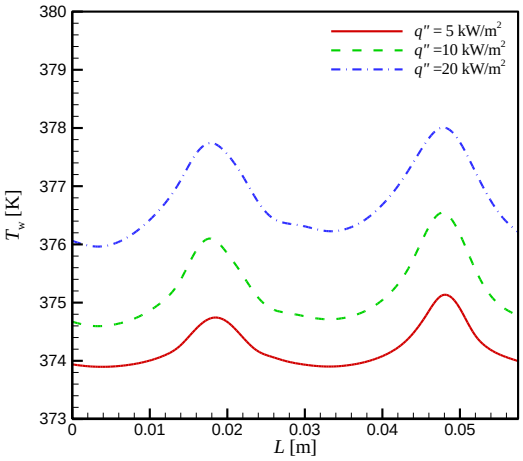
380
379
378
377
376
375
374
373
T_w [K]
0
0.01
0.02
0.03
0.04
0.05
L [m]
q'' = 5 kW/m^2
q'' =10 kW/m^2
q'' =20 kW/m^2

Figure 13

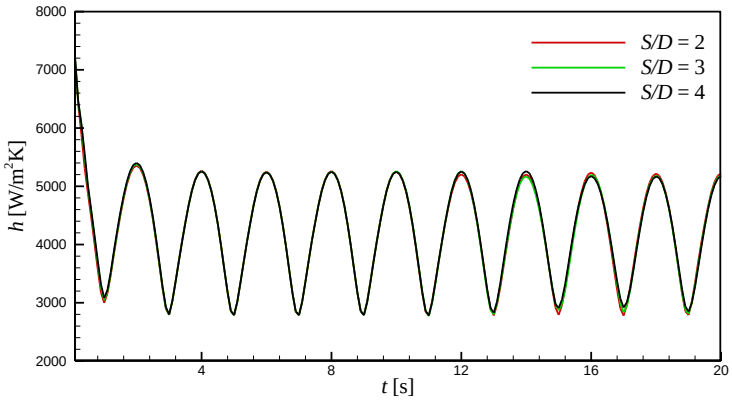

(a)

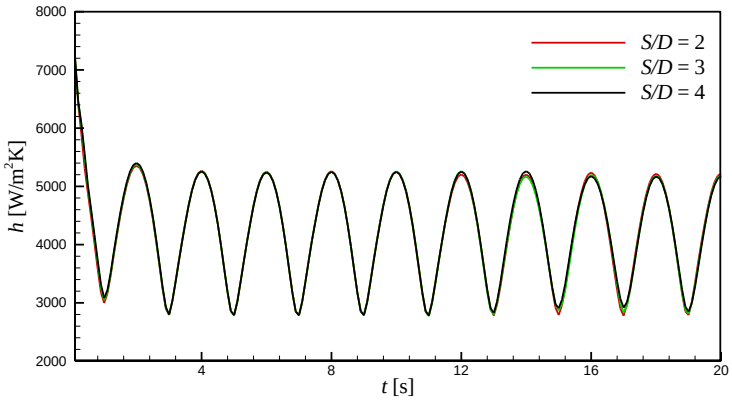

(b)

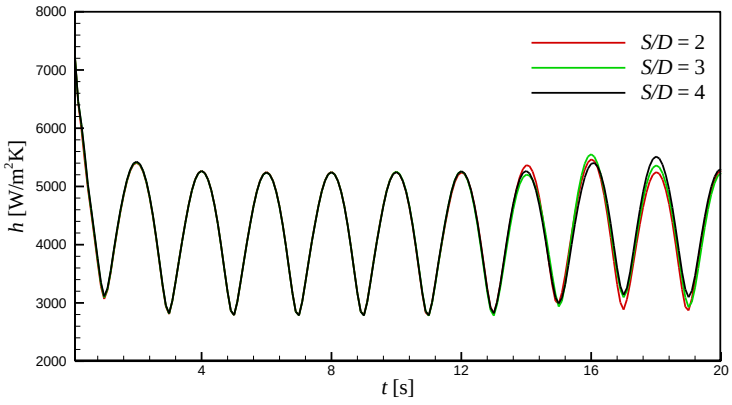

(c)

Figure 14

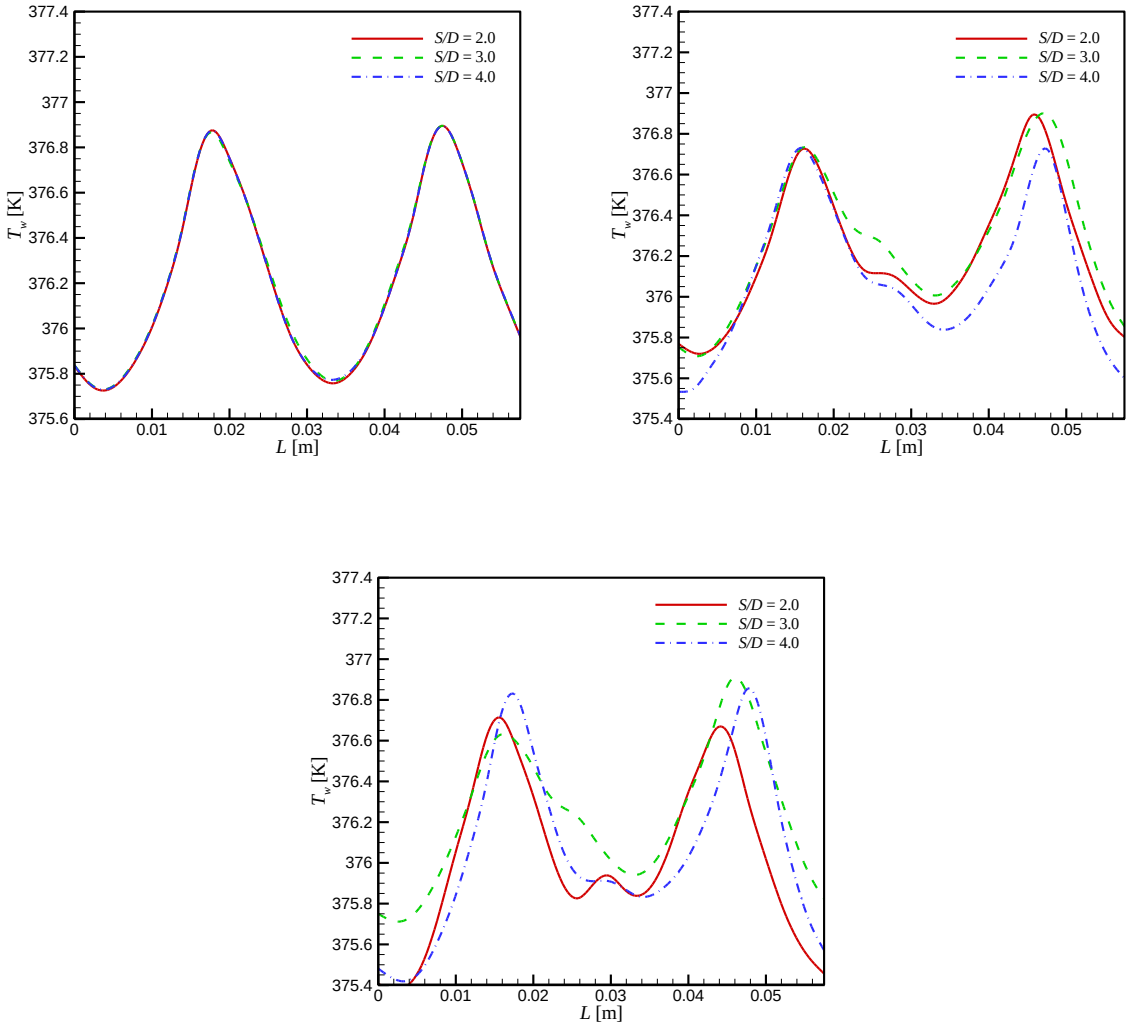

Figure 15

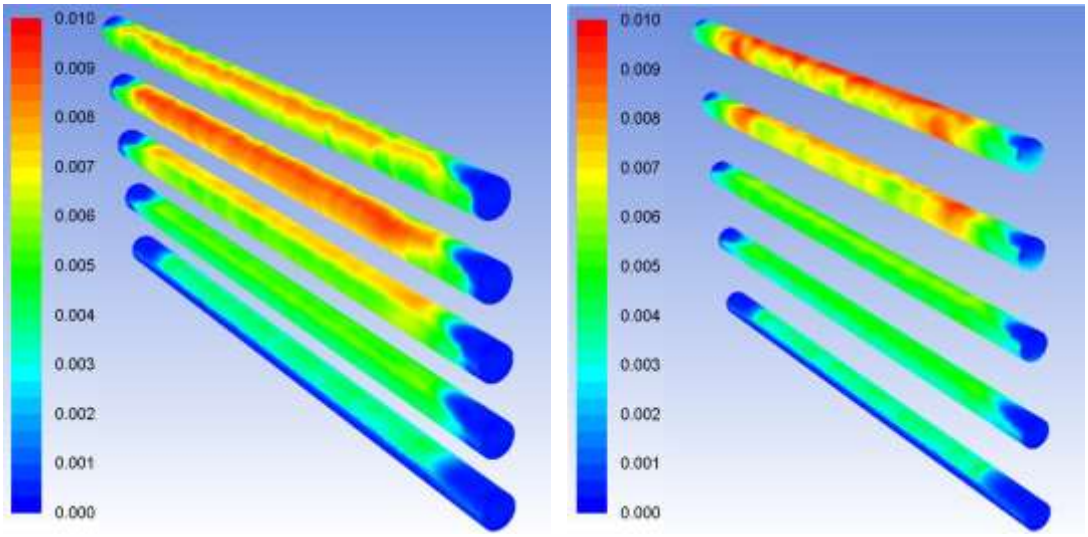

(a) (b)

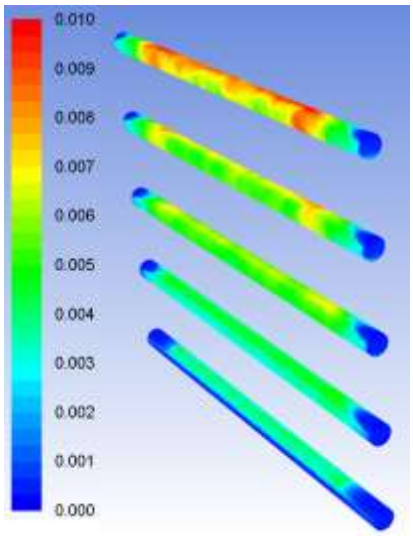

(c)

Figure 16

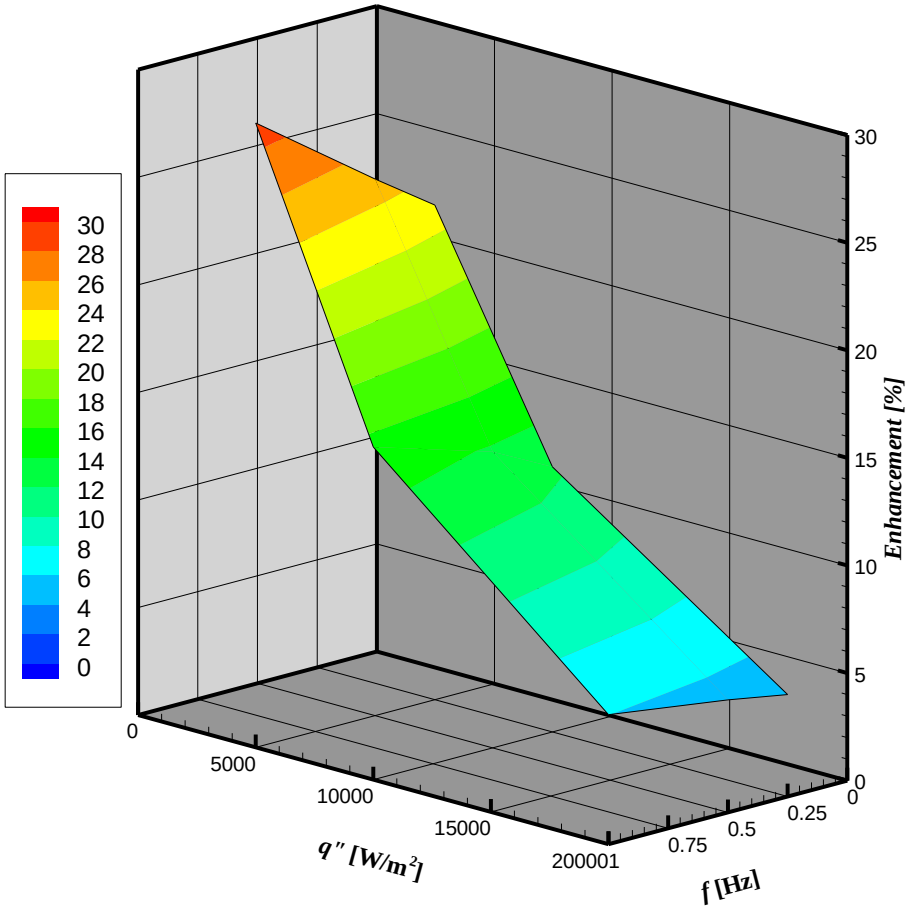
30
28
26
24
22
20
18
16
14
12
10
8
6
4
2
0
0
5000
10000
15000
200001
q'' [W/m²]
0
0.25
0.5
0.75
f [Hz]
0
5
10
15
20
25
30
Enhancement [%]

Figure 17

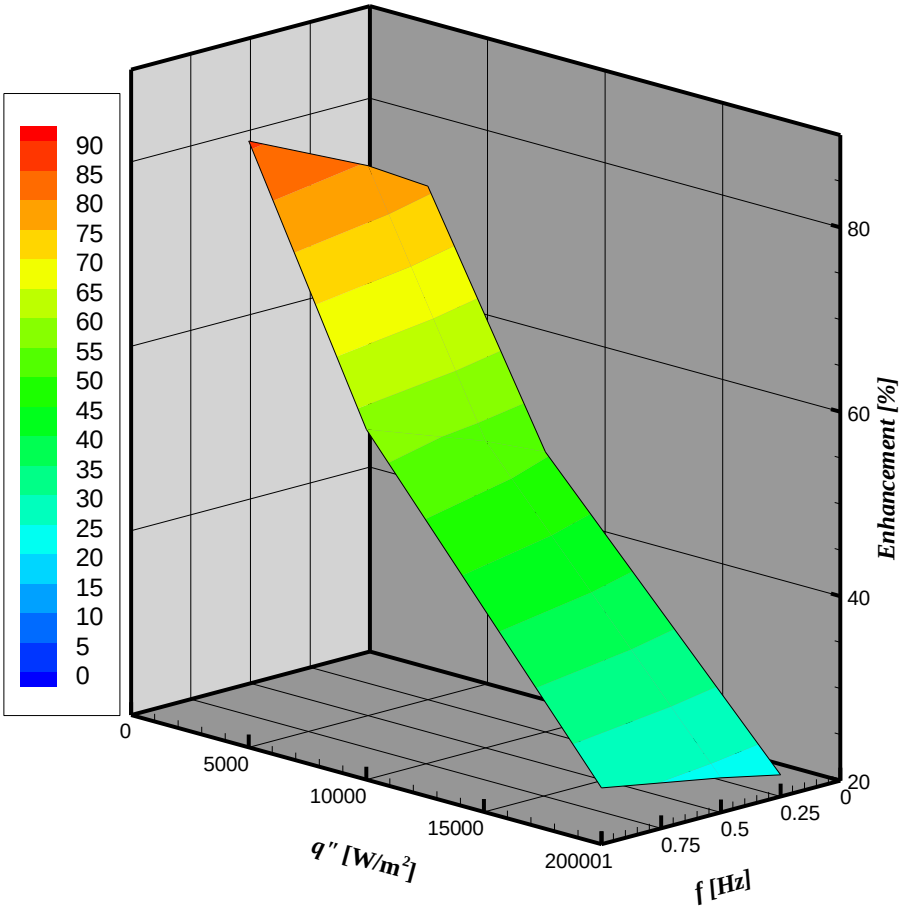
90
85
80
75
70
65
60
55
50
45
40
35
30
25
20
15
10
5
0
0
5000
10000
15000
200001
q'' [W/m²]
0
0.25
0.5
0.75
f [Hz]
20
40
60
80
Enhancement [%]

Figure 18

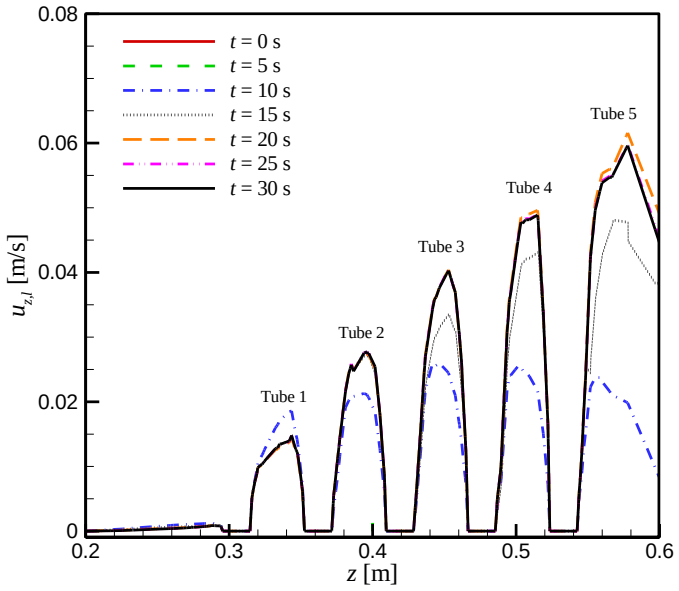
0.08
0.06
0.04
0.02
0
0.2
0.3
0.4
0.5
0.6
$u_{z,l}$ [m/s]
z [m]
t = 0 s
t = 5 s
t = 10 s
t = 15 s
t = 20 s
t = 25 s
t = 30 s
Tube 1
Tube 2
Tube 3
Tube 4
Tube 5

Figure 19

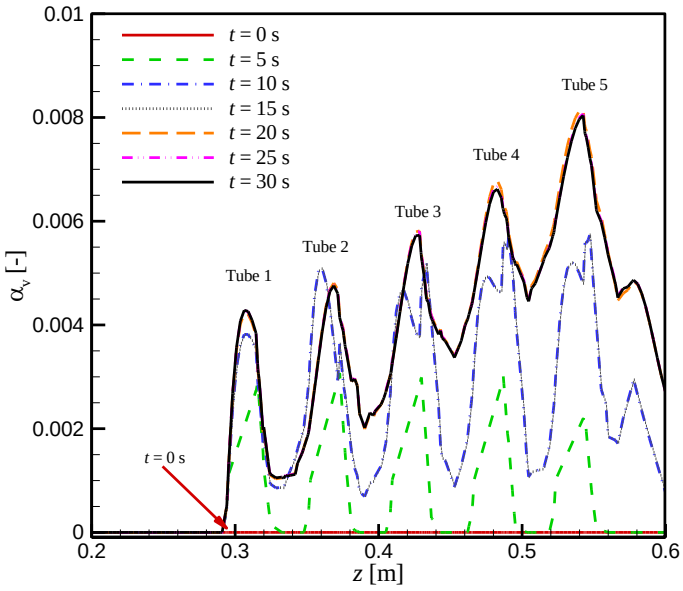
0.01
0.008
0.006
0.004
0.002
0
0.2
0.3
0.4
0.5
0.6
α_v [-]
z [m]
t = 0 s
t = 5 s
t = 10 s
t = 15 s
t = 20 s
t = 25 s
t = 30 s
Tube 1
Tube 2
Tube 3
Tube 4
Tube 5
t = 0 s

Figure 20

Tables:

Table 1

(a) Effect of U_m (f = 1 Hz, S/D = 2, q'' = 10 kW/m^2)

U_m (m/s)	0.2	0.5	1
ER (%)	15.46	57.99	128.81

(b) Effect of q'' (U_m = 0.2 m/s, f = 0.5 Hz, S/D = 3)

q'' (kW/m^2)	5	10	20	50	100
ER (%)	24.94	13.76	5.23	1.13	0.19

(c) Effect of S/D (U_m = 0.2 m/s, f = 0.5 Hz, q'' = 10 kW/m^2)

S/D (-)	2	3	4	5	6
ER (%)	13.22	13.81	13.84	13.83	13.84

(d) Effect of f (U_m = 0.2 m/s, S/D = 3, q'' = 10 kW/m^2)

f (Hz)	0.25	0.5	1	2	10	15	20
ER (%)	12.32	13.76	15.46	19.45	19.87	20.36	20.22

Table 2

Parameter	Range
f **(Hz)**	0.25–1.0
U_m **(m/s)**	0.2–0.5
S/D **(-)**	2–4
q'' **(W/m^2)**	5–20

Research highlights

I. An increase of up to 90% in the heat transfer coefficient can be achieved through the vibrations caused by a forced fluid motion induced by surface boiling.

II. The heat transfer rate increases with the frequency/amplitude of the mechanical vibration.

III. The enhancing effect of the vibration is most vigorous for moderately low heat fluxes.

IV. The pitch-to-diameter ratio has a negligible effect on the enhancing effect of a vibration.

V. It is found that the optimum frequency of the vibration is 2 Hz for the simulated operating conditions.